



Development of antiviral carbon quantum dots that target the Japanese encephalitis virus envelope protein

Received for publication, January 1, 2022, and in revised form, April 6, 2022. Published, Papers in Press, April 20, 2022.
<https://doi.org/10.1016/j.jbc.2022.101957>

Han-Hsiang Chen¹, Chin-Jung Lin², Anisha Anand², Han-Jia Lin^{2,3}, Hung-Yun Lin², Ju-Yi Mao², Pei-Hua Wang⁴, Yufeng Jane Tseng^{4,5}, Wen-Shyong Tzou² , Chih-Ching Huang^{2,3,6,*} , and Robert Y. L. Wang^{1,7,8,9,*} 

From the ¹Division of Microbiology and Immunology, Graduate Institute of Biomedical Sciences, College of Medicine, Chang Gung University, Taoyuan, Taiwan; ²Department of Bioscience and Biotechnology, and ³Center of Excellence for the Oceans, National Taiwan Ocean University, Keelung, Taiwan; ⁴Graduate Institute of Biomedical Electronics and Bioinformatics, and ⁵Department of Computer Science and Information Engineering, National Taiwan University, Taipei, Taiwan; ⁶School of Pharmacy, College of Pharmacy, Kaohsiung Medical University, Kaohsiung, Taiwan; ⁷Department of Biomedical Sciences, College of Medicine, Chang Gung University, Taoyuan, Taiwan; ⁸Division of Pediatric Infectious Diseases, Department of Pediatrics, Chang Gung Memorial and Children's Hospital, Linkou, Taiwan; ⁹Kidney Research Center and Department of Nephrology, Chang Gung Memorial Hospital, Linkou, Taiwan

Edited by Craig Cameron

Japanese encephalitis is a mosquito-borne disease caused by the Japanese encephalitis virus (JEV) that is prevalent in Asia and the Western Pacific. Currently, there is no effective treatment for Japanese encephalitis. Curcumin (Cur) is a compound extracted from the roots of *Curcuma longa*, and many studies have reported its antiviral and anti-inflammatory activities. However, the high cytotoxicity and very low solubility of Cur limit its biomedical applications. In this study, Cur carbon quantum dots (Cur-CQDs) were synthesized by mild pyrolysis-induced polymerization and carbonization, leading to higher water solubility and lower cytotoxicity, as well as superior antiviral activity against JEV infection. We found that Cur-CQDs effectively bound to the E protein of JEV, preventing viral entry into the host cells. In addition, after continued treatment of JEV with Cur-CQDs, a mutant strain of JEV was evolved that did not support binding of Cur-CQDs to the JEV envelope. Using transmission electron microscopy, biolayer interferometry, and molecular docking analysis, we revealed that the S123R and K312R mutations in the E protein play a key role in binding Cur-CQDs. The S123 and K312 residues are located in structural domains II and III of the E protein, respectively, and are responsible for binding to receptors on and fusing with the cell membrane. Taken together, our results suggest that the E protein of flaviviruses represents a potential target for the development of CQD-based inhibitors to prevent or treat viral infections.

Viruses are responsible for more than 30% of deaths from infectious diseases (1). For example, COVID-19, an emerging infectious disease caused by severe acute respiratory syndrome coronavirus 2 (SARS-CoV-2), has infected over 417 million people worldwide and caused more than 6 million deaths as of March 2022. Therefore, there has been a dramatic increase in

the demand for antiviral agents to combat viral infections. However, the development of new antiviral drugs requires considerable time and several stages before they can be approved for human use. Therefore, the development of innovative, long-term, and highly flexible drugs with virostatic and/or virucidal properties to complement existing pharmacological approaches against viral infection and transmission is essential. Many nanomaterials have been shown to exhibit intrinsic antiviral activities (2–6). Although some metal, metal oxide, and semiconductor nanoparticles have potent antiviral activities, their biocompatibility remains a concern (7–10). Recently, low cytotoxic carbon-based nanomaterials such as graphene oxides (GOs), carbon nanotubes (CNTs), fullerenes, and carbon quantum dots (CQDs) have shown promising antiviral effects (11–13). For example, GO can inactivate DNA and RNA viruses by direct physical damage to the viral structure through the sharp edges of GO (14, 15). Fullerenes and their derivatives inhibit human immunodeficiency virus (HIV) by inhibiting HIV proteases, reverse transcriptase, or DNA polymerases (16). In addition to HIV, fullerene derivatives have been reported to inhibit hepatitis C virus, herpes simplex virus, respiratory syncytial virus, Zika virus (ZIKV), and influenza virus (17–21). In contrast to inactivated viruses, CNTs are incorporated into filtration systems for the removal of viral particles (22).

The highly tunable surface properties of CQDs confer different antiviral capabilities compared to GO, CNT, and fullerenes (13, 23–27). CQDs are small-sized carbon nanomaterials (typically smaller than 10 nm) with good water dispersion, remarkable optical properties (intense and excitation-dependent emission), extreme (photo) stability, and high biocompatibility (28). Numerous CQDs synthesized by hydrothermal and pyrolytic methods from different precursors have been developed as antiviral agents against HIV, herpes simplex virus, respiratory syndrome virus, pseudorabies virus, porcine epidemic diarrhea virus, human coronavirus, and enterovirus (13, 23–27). Compared to other antiviral

* For correspondence: Robert Y. L. Wang, yuwang@mail.cgu.edu.tw; Chih-Ching Huang, huangcing@ntou.edu.tw.

Antiviral CQDs targeting the JE viral envelope protein

nanomaterials, the highly flexible CQDs from different precursors confer their ability to fight various viruses. The precursor molecules residing on CQDs are mainly responsible for their antiviral effects. Although many antiviral mechanisms have been proposed for CQDs, such as preventing viral particles from attaching to host cells, inhibiting viral replication, and stimulating innate immune response, most reported CQDs interfere with the attachment and penetration steps through direct contact between CQDs and viral membranes (13, 23–27). Even so, the mechanism of binding of CQDs to viral particles is still far from being fully understood.

We previously reported that CQDs derived from curcumin (Cur) exhibited superior antiviral activity against enterovirus 71 (13). However, the antiviral mechanism of Cur-CQDs is unclear, even though we proposed the CQDs bind mainly to virions and prevent them from attaching to host cells. In this work, we sought to achieve antiviral potency of Cur-CQDs against another virus, Japanese encephalitis virus (JEV), and to provide direct insight into the interaction between CQDs and virions. Japanese encephalitis has become one of the serious health problems in tropical and subtropical regions of the world, with high mortality and neurological complications in patients even after recovery (29). JEV, an enveloped flavivirus, is the leading cause of viral encephalitis in Asia, with an estimated 70,000 clinical cases per year (30). Currently, there is no effective antiviral treatment for JEV, and patients can only be provided with supportive therapy to relieve symptoms. As with other flaviviruses, once JEV enters the host cell *via* endocytosis, the surface envelope (E) protein of the virion plays a central role in mediating the process of fusion of the viral envelope with the endosomal membrane at low pH. As a result, the genome is released into the cytoplasm, which then completes the steps of replication, assembly, and egress of the JEV. In this study, the antiviral Cur-CQDs were obtained by pyrolysis of Cur at 180 °C for 2 h. Cur-CQDs exhibited superior solubility (50 mg ml⁻¹) in an aqueous solution

compared to Cur (<10⁻² mg ml⁻¹). Cur-CQDs showed inhibition of JEV infection in pretreatment and cotreatment and were found to bind to host cell membrane as well as viral particles to inhibit the virus. However, inhibition of viral infection was mainly achieved by binding to viral particles, preventing infection even at the early stages of virus entry. Another interesting aspect of the present study is that cotreatment of JEV with Cur-CQDs produced a JEV mutant with low infectivity and cytopathological properties. Furthermore, in the present study, the major binding sites of Cur-CQDs to envelope (E) proteins have been identified by quasispecies genome-like sequencing, binding affinity measurements and *in silico* molecular docking. JEV E protein promotes cell attachment and membrane fusion and is considered to be the main targets of neutralizing inhibitors (31). Thus, our results suggest that Cur-CQDs may be a promising agent for the prevention of JEV infection.

Results

The establishment of Cur CQDs

First, we synthesized new Cur carbon nanoparticles, called Cur-CQDs. The pyrolysis of Cur forms Cur-CQDs mainly through sequential dehydration, polymerization, cross-linking, and partial carbonization. Well-stacked Cur molecules in the solid-state undergo dehydration condensation, followed by the formation of polymerized Cur. The polymerized Cur is condensed and polymerized into macromolecular polymers, followed by partial carbonization at temperature (180 °C) and an increase in the size of the carbon core (Fig. 1A). The as-formed Cur-CQDs were then purified by dialysis and freeze-drying to determine the yield. The Cur-CQDs were subsequently analyzed using transmission electron microscopy (TEM) and high-resolution TEM, the average size of the prepared Cur-CQDs was about ca. 4.8 nm, exhibiting typical carbon dot core crystals and optical properties (Fig. 1B). The

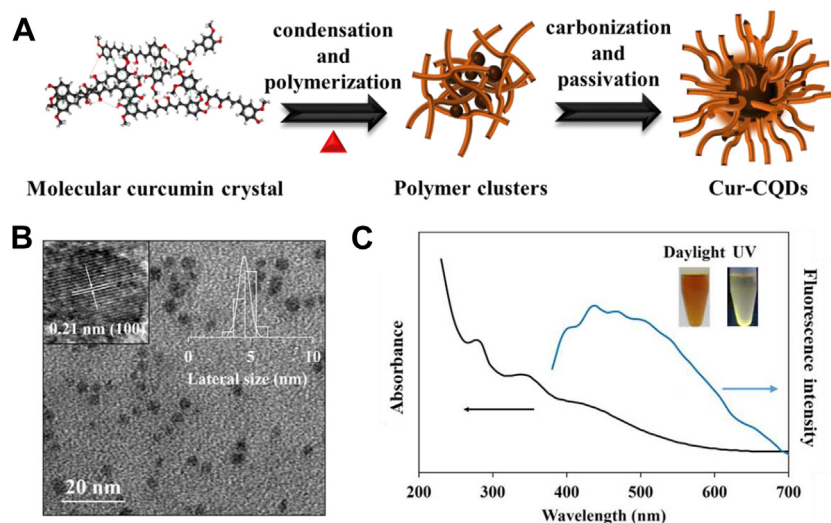


Figure 1. The synthesis of Cur-CQDs. A, schematic representation of the formation mechanism of Cur-CQDs. B, transmission electron microscopy (TEM) and high-resolution TEM (HRTEM) images and (C) UV-vis absorption and fluorescence spectra images of as-prepared Cur-CQDs. Inset to (B): HRTEM and size distribution of the CQDs. Inset to (C): photograph of the color and fluorescence of the CQDs under daylight and upon excitation under a hand-held UV lamp (365 nm), respectively. Cur-CQDs, Curcumin carbon quantum dots.

pyrolytic products of polymeric Curs are anchored on the surfaces of the Cur-CQDs to form polymeric dot structures and exerting enhanced activities of Cur. The UV-Vis absorption and fluorescence spectra of Cur-CQDs are shown in Figure 1C. The Cur-CQDs has an absorption band at 285 nm is ascribed to the $\pi \rightarrow \pi^*$ transitions of conjugated C=C bonds, supporting the formation of graphitic carbon cores in the Cur-CQDs (32). The Cur-CQDs also showed a shoulder band at 3–0–360 nm can be attributed to the $n \rightarrow \pi^*$ transitions of C=O bonds or interlayer $\pi \rightarrow \pi^*$ charge transfer (33).

Cur-CQDs have low cytotoxicity and low reactive oxygen species formation in BHK-21 cells

Several studies have reported the Cur is high cytotoxic and has many interference properties (34, 35); however, when Cur was modified into nanoparticles, it reduced its toxicity to cells and increased its antiviral activity (36, 37). To examine the toxicity of the prepared Cur-CQDs to cells and to compare them with the Cur (native form), we added different concentrations (1, 10, 30, 50, 100, 500, and 1000 $\mu\text{g ml}^{-1}$) of Cur or Cur-CQDs to BHK-21 cells for 24 h and analyzed the cell viability by MTT assay. The results revealed that Cur was highly toxic to BHK-21 cells, with cell survival rates below 10% even at concentrations as low as 10 $\mu\text{g ml}^{-1}$ (Fig. S1, Supporting information). In contrast, the cell survival rate of BHK-21 cells treated with Cur-CQDs was still higher than 80% at concentrations as high as 100 $\mu\text{g ml}^{-1}$, indicating the high biocompatibility of Cur-CQDs (Fig. S1, Supporting information). We were surprised to find that the half-maximal cytotoxicity concentration values of Cur-CQDs were at least 50-fold higher than those of Cur. It is well known that Cur induced apoptosis mainly due to the production and subsequent induction of reactive oxygen species (ROS), instability of mitochondrial transmembrane, down-regulation of Bcl-2 and IAP family proteins, release of cytochrome c, and activation of caspases (38). Therefore, to understand whether Cur-CQDs promote ROS formation, we

used a 2'-7'-dichlorofluorescein diacetate (DCFH-DA) assay. From the results, we found that Cur-CQDs produced at least 5-fold less ROS than Cur (Fig. S2, Supporting information).

Cur-CQDs inhibit the JEV infection by affecting the early steps of viral infection

To assess the inhibitory effect of Cur-CQDs on JEV infection, we performed three different experiments (pretreatment, cotreatment, and posttreatment) (Fig. 2A). In pretreatment, BHK-21 cells were treated with Cur-CQDs and then infected with JEV and cultured to assess infection. In cotreatment, the mixture of preincubated JEV and Cur-CQDs was added to the cell cultures and then cultured for 24 h. Posttreatment was performed by infecting cells with JEV followed by the addition of Cur-CQDs. In the cotreatment approach, viral RNA production and protein levels of viral nonstructural protein 5 (NS5) and nonstructural protein 3 (NS3) showed a significant decrease (Fig. 2C). The flaviviral proteins NS5 and NS3 are the two largest proteins of JEV and play important roles in the life cycle of the virus (39, 40). The N-terminal and C-terminal structural domains of NS5 are critically involved in viral cap formation and genome replication, respectively (40). Meanwhile, NS5 recognizes the nuclear transporter of importin α/β and importin β 1 for nuclear localization to produce virus (41). On the other hand, NS3 protein plays an important role in processing viral polyprotein and replication by regulating the activities of protease, helicase, and nucleoside 5'-triphosphatase (42). However, the inhibition of viral RNA and protein levels by Cur-CQDs was much weaker in the pretreatment and posttreatment than cotreatment (Fig. 2, B–D). In this study, in addition to Cur-CQDs inhibiting the JEV infected to BHK-21 cells (Fig. 2), it also inhibited JEV infection of other cell lines, HEK-293T (human embryonic kidney cell) and Vero cells (monkey kidney epithelial cell), confirming their superior antiviral efficacy against JEV (Fig. S3, Supporting information). The half-maximal inhibitory concentration (IC_{50}) of Cur-CQDs in cotreatment (0.9 $\mu\text{g ml}^{-1}$) was 100-fold lower than

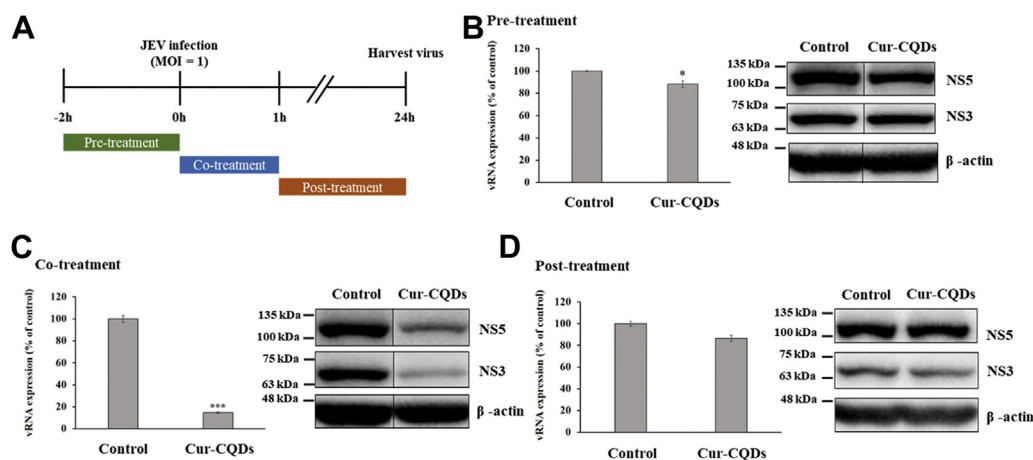


Figure 2. Cur-CQDs inhibit JEV infection. A, schematic diagram of the dosing time experiments to assess the antiviral activity of Cur-CQDs (100 $\mu\text{g ml}^{-1}$). JEV infection of BHK-21 cells (MOI=1) by (B) pretreatment, (C) cotreatment, and (D) posttreatment assays in the presence of Cur-CQDs was determined by Western blot and RT-qPCR analysis. Error bars represent the standard deviation of three independent measurements. Please note that the images in Figure 2, B and C were from the same gel with the splice point indicated. Asterisks indicate the statistically significant differences in the treatment groups compared to the control group (* $p < 0.05$; *** $p < 0.001$). Cur-CQDs, Curcumin carbon quantum dots.

Antiviral CQDs targeting the JE viral envelope protein

in pretreatment ($>100 \mu\text{g ml}^{-1}$; incubation of CQDs and BHK-21 cells was performed at 4°C), further supporting the effect of Cur-CQDs on JEV (Fig. S4A, Supporting information). Meanwhile, addition of Cur-CQDs ($100 \mu\text{g ml}^{-1}$) immediately prior to infection of BHK-21 cells with JEV (MOI=1) without removal of Cur-CQDs showed similar antiviral activity as in the cotreatment experiments (premixed JEV and Cur-CQDs, followed by infection of BHK-21 cells). The IC_{50} of Cur-CQDs to inhibit the virus in a cotreatment manner was much lower than most reported antiviral carbon-based nano-materials (24, 26, 43–45). This suggests that the antiviral activity of Cur-CQDs is mainly through the inhibition of the early steps of the viral infection, which may be the mechanism of viral attachment and entry.

Cur-CQDs bind mainly to viral particles and inhibit JEV infection

Since the antiviral activity of Cur-CQDs is due to the inhibition of early viral infection stages, we further elucidated that the antiviral effect is due to the binding of Cur-CQDs to viral particles or host cell membranes. The pretreatment assay was performed at 37°C or 4°C to understand the binding between Cur-CQDs and host cells or viruses. Cur-CQDs were added to cell cultures and incubated at 37°C or 4°C for 2 h, followed by infection with JEV for 8 h or 24 h. The results of RT-qPCR analysis showed a reduction in viral RNA under pretreatment at 37°C and after 8 h or 24 h of infection (Fig. 3A). However, a more significant reduction of about 40% in viral RNA was observed with pretreatment at 4°C (Fig. 3B). Therefore, we hypothesized that Cur-CQDs would attach to the cell membrane at 4°C and prevent viral particles from binding to the cell, thereby inhibiting virus infection. However,

cotreatment exhibited $>95\%$ inhibition (Fig. 3C), indicating that Cur-CQDs bound to JEV contributed significantly to viral inhibition. The interaction between Cur-CQDs and JEV was supported by TEM. TEM images of JEV after incubation with Cur-CQDs showed the presence of characteristic lattice fringes of CQDs on the surface of JEVs, implying that CQDs bind to the virus surface to exert antiviral effects (Fig. 4A).

Cur-CQDs interact with specific sites of E protein to inhibit the entry of JEV on host cells

Our results have shown that the Cur-CQDs can effectively bind to the JEV surface to prevent its attachment and/or entry into the host cell. Next, we sought to determine the location of the JEV virions to which Cur-CQDs were attached. To understand the site of binding of JEV to Cur-CQDs, we performed a virus adaptation test. Consecutive passages of JEV were performed in the presence of Cur-CQDs, and resistant quasispecies of JEV were selected after 12 passages. After BigDye terminator sequencing of the obtained mutant viruses, nonsynonymous mutations in the JEV genome resulted in amino acids substitutions from serine (S) to arginine (R) at position E 123 and from lysine (K) to arginine (R) at position E 312 (Table S1, Supporting information). Only two mutation sites, S123R and K312R, were found in the E protein, hence named JEV E-S123R/K312R (Fig. 5A). Therefore, we hypothesized that JEV E-S123R/K312R is more resistant to Cur-CQD than WT JEV. The IC_{50} of Cur-CQDs against JEV E-S123R/K312R strain ($>100 \mu\text{g ml}^{-1}$; Fig. S4B) was much higher than that of the WT one ($0.9 \mu\text{g ml}^{-1}$) (Fig. S4A), further supporting the Cur-CQDs' weak inhibitory activity against the mutant strain. Compared to WT JEVs (Fig. 4A), Cur-CQDs were not observed on the surface of JEV E-S123R/K312R, indicating the

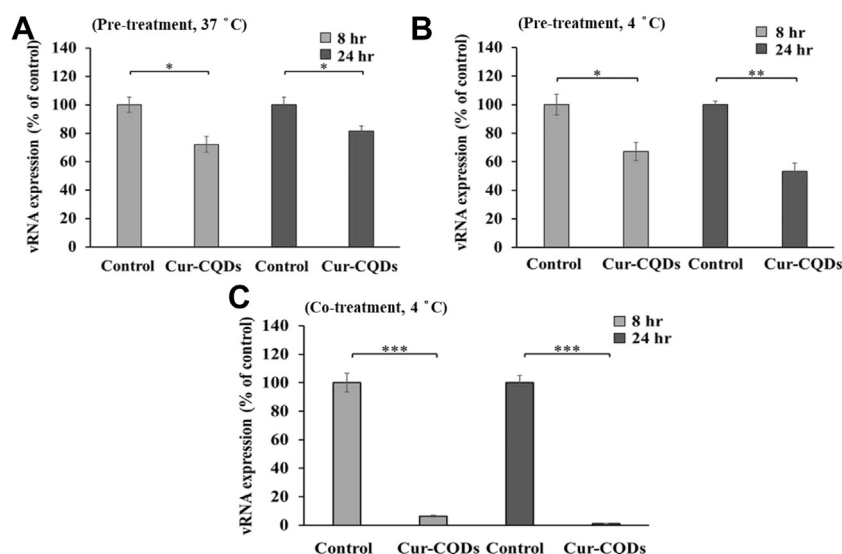


Figure 3. Cur-CQDs bound to cell membranes or viral particles to inhibit infection. Viral RNA expression assay of BHK-21 cells pretreated with Cur-CQDs and then infected with JEV or cotreated with the mixture of JEV and Cur-CQDs. The Cur-CQDs were incubated with BHK-21 cells at (A) 37°C and (B) 4°C for 2 h and then washed twice with PBS before pretreatment for JEV infection. C, BHK-21 cells were incubated with a mixture of preincubated JEVs and Cur-CQDs for 2 h at 4°C cotreatment assays. The infected cells from the pretreatment and cotreatment were further incubated for 8 or 24 h and then subjected to RT-qPCR analysis to detect the amount of viral RNA. Error bars represent the standard deviation of three independent measurements. Asterisks indicate the statistically significant difference in treated groups compared to the uninfected control group (* $p < 0.05$; ** $p < 0.01$; *** $p < 0.001$). Cur-CQDs, Curcumin carbon quantum dots; JEV, Japanese encephalitis virus.

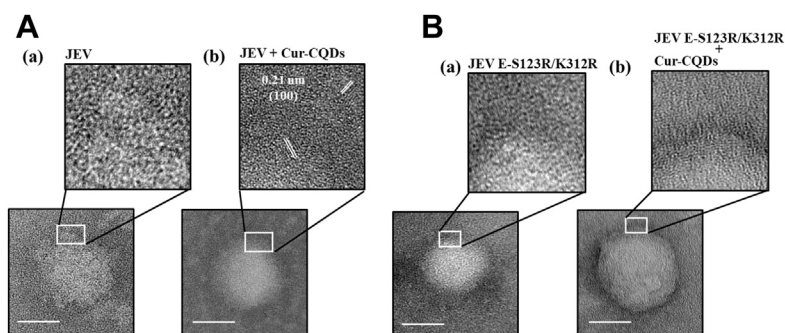


Figure 4. Cur-CQDs binds the JEV particles. TEM images of (A) JEV (2×10^8 PFU ml^{-1}) and (B) JEV E-S123R/K312R (2×10^8 PFU ml^{-1}) mutant virus in the (a) absence and (b) presence of Cur-CQDs ($10 \mu\text{g ml}^{-1}$). A-b, Cur-CQDs were detected surrounding the JEV particle surface in the presence of Cur-CQDs compared to the environment in which (A-a) Cur-CQDs are not present. B-b, In the presence of Cur-CQDs, Cur-CQDs do not adsorb around the surface of JEV E-S123R/K312R particle, which is exactly the same as (B-a) JEV E-S123R/K312R viral particle in the absence of Cur-CQDs. Scale bar: 10 nm. Cur-CQDs, Curcumin carbon quantum dots; JEV, Japanese encephalitis virus.

effect of Cur-CQDs binding directly to the E-S123/K312 site (Fig. 4B). Cotreatment experiments and TEM results supported the possibility that Cur-CQDs may interact with specific sites of E protein to inhibit the attachment and fusogenic effect of JEV on host cells.

Cur-CQDs binds directly to the E-S123/K312 sites of the E protein through the guaiacol

Our previous reports showed that Cur-CQDs have a large number of 4-vinyl guaiacol moieties on their surface, which was demonstrated in laser desorption/ionization time-of-flight mass spectrometry (13). Furthermore, by systematically investigating the antiviral potency of Cur and its derivatives, such as bis-demethoxycurcumin, demethoxycurcumin, and tetramethylcurcumin (FLLL31), some reports have suggested that guaiacol is mainly responsible for the antiviral activities against

flaviviruses (46–48). Therefore, molecular docking of guaiacol with WT E and E-S123R/K312R proteins was stimulated by Schrodinger software using the exhaustive binding mechanism of Cur-CQDs to JEV. Given the strong influence of S123R and K312R on the binding of Cur-CQDs, we attempted to dock these two positions and found binding sites. Residue S123 and K312 were located in domains II and III of the ectodomain of the E protein (Fig. S5, Supporting information). In domain II, the methoxy and hydroxyl groups of guaiacol were surrounded by residues 61, 123 to 128, and 205 to 207 of the E protein (Fig. S6A, Supporting information). The phenolic group is predicted to be the hydrogen bond donor for the K124 side chain (1.87 \AA) and the hydrogen bond acceptor for the G207 (1.82 \AA) and Y61 (1.92 \AA) side chains on the anti-parallel β -sheet. These three hydrogen bonds allow guaiacol to bind tightly to domain II of the E protein. The other docking site with domain III shows a cavity that allows guaiacol to form a

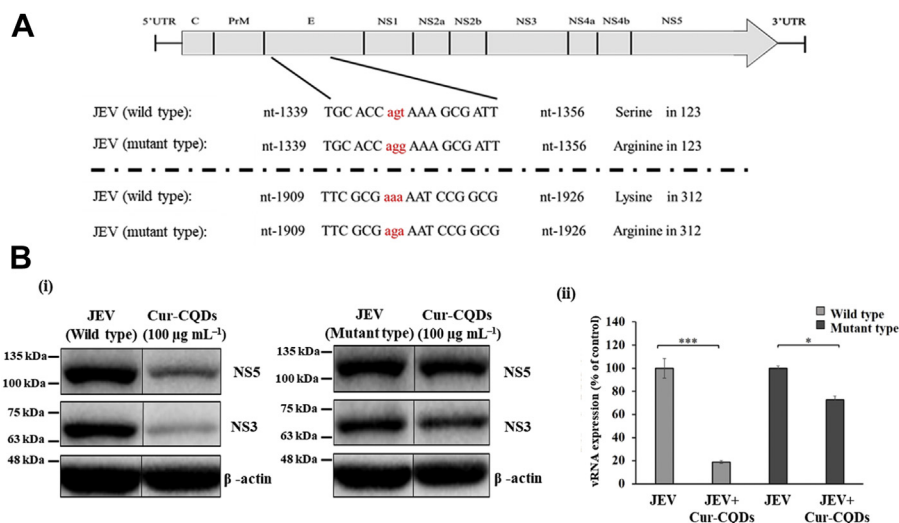


Figure 5. Quasispecies of JEV resistant to Cur-CQDs. Consecutive passages of JEV were performed in the presence of Cur-CQDs, and resistant quasispecies of JEV were selected after 12 passages. A, mutation location analysis of JE virus sequences after 12 passages in the presence of Cur-CQDs confirmed that only two mutation sites, S123R and K312R, were found in the E protein. B, antiviral effect of Cur-CQDs ($100 \mu\text{g ml}^{-1}$) on WT and mutant JEV by Western blotting (i) and qRT-PCR analysis (ii). Note that the images in Figure 5B (i) were from the same gel with the splice point indicated. The experimental procedure and conditions of Figures 2C and 5B (i) are identical. We have carried out this experimental procedure at least four times independently, and the experimental conclusions remain the same. After comparison, the best Western blotting data are presented by Figure 2C, so we reuse Figure 2C in this panel for the same condition. Error bars indicating the standard deviation for three experimental replicates. (* $p < 0.05$; *** $p < 0.001$). Cur-CQDs, Curcumin carbon quantum dots; JEV, Japanese encephalitis virus.

Antiviral CQDs targeting the JE viral envelope protein

hydrogen bond donor with S149 (1.69 Å) (Fig. S6B, Supporting information). In addition, the residue located at K312 (4.97 Å) possesses a Pi-cation interaction with the aromatic ring on guaiacol to stabilize its spatial position. The binding energies of guaiacol located in two docking positions of domains II and III were calculated to be -4.746 and -3.446 kcal mol⁻¹, indicating that the salt-bridge effect near S123 is significantly stronger than that of K312 (Table S2, Supporting information). The distance between these two regions (5.52 nm) is shorter than the hydrodynamic size of Cur-CQDs (13.6 nm), resulting in a polymeric surface structure of Cur-CQDs with dense guaiacol moieties that can bind strongly and multivalently to E protein by docking S123 and K312 regions.

In the molecular docking analysis, the distances of the two docking sites S123 and K312 (magenta color) from the receptor binding domain (orange color) were 64.34 and 12.40 Å (Fig. S5), respectively, which is close to the diameter of Cur-CQDs (48.00 Å). It is conceivable that Cur-CQDs could neutralize E protein to hinder viral endocytosis when they bind to E protein. Furthermore, considering that residue S123 located in domain II and residue K312 located in domain III are adjacent to the fusion loop and stem region, respectively, we speculated that the spatial barrier also limits the trimerization of E protein during fusion after binding to Cur-CQDs. The molecular docking model also simulated the binding of two mutated sides (E-S123R and E-K312R). As a result of the E-S123R mutation, the hydroxyl side chain of the amino acid was replaced by a guanidinium group, leading to a significant change in the microstructure. The relative spatial position of Y61 was pushed outward by residue S123R, resulting in an

increased distance to guaiacol (2.18 Å) and subsequent loss of hydrogen bonding (Fig. S6C, Supporting information). The docking site R312 of the E-K312R protein was replaced by arginine, so the lysine side chain and guaiacol were lost in the spatial position (Fig. S6D, Supporting information). Due to the loss of the cavity structure, the Pi-cation interaction of guaiacol and K312 was also lost. The binding energies of the two single mutants, E-S123R and E-K312R, were reduced to -4.380 and -2.583 kcal mol⁻¹, respectively (Table S2, Supporting information).

The molecular docking results showed that the binding site of guaiacol and E-protein was mainly through hydrogen bonding and Pi-cation interactions, and the binding affinities of the two mutant regions was weak. To validate the *in silico* molecular docking analysis, we expressed JEV WT, single mutant (S123R and K312R) and double mutant (S123R/K312R) E proteins and performed biolayer interferometry to measure their binding affinity. The dissociation constant (K_d) of Cur-CQDs with WT E, E-S123R, E-K312R, and E-S123R/K312R were determined to be 9.58×10^{-9} , 7.64×10^{-8} , 2.19×10^{-8} , and 1.26×10^{-6} (g L⁻¹), respectively, showing that CQDs exhibited much weak binding affinity for the double mutant E-S123R/K312R (Fig. 6). As predicted by the docking model, mutation of neutral serine to basic arginine (E-S123R) resulted in a greater decrease in binding strength to Cur-CQDs (K_d 7.64×10^{-8} versus 2.19×10^{-8} M) compared to mutation of basic lysine to basic arginine (E-K312R). The K_d value of the double mutant E-S123R/K312R was more than 15-fold higher than E-K312R and E-S123R, suggesting that both residues of E-S123/K312 play an important role in the interaction with

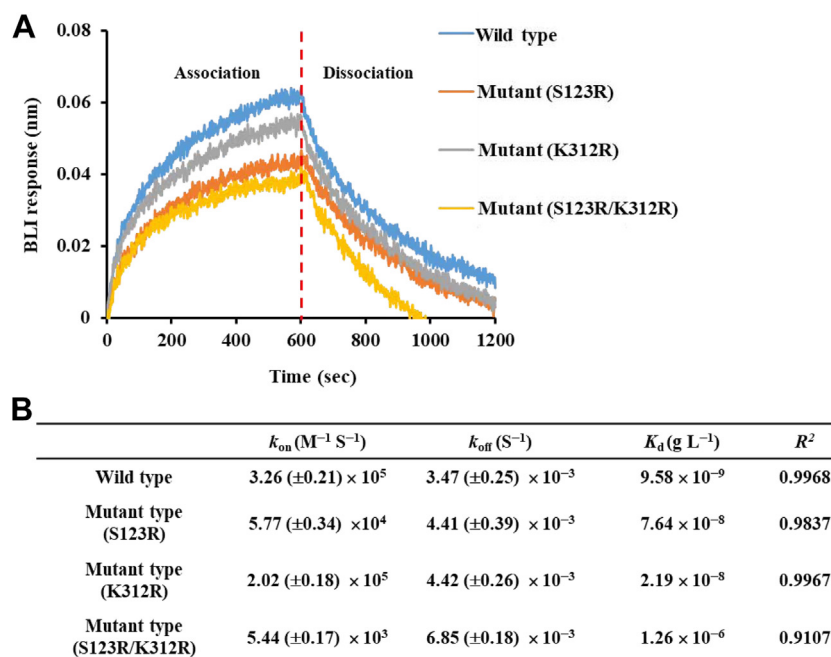


Figure 6. Binding affinity of Cur-CQDs to WT and mutant JEV E proteins. Three recombinant JEV WT, single mutant (S123R and K312R), and double mutant (S123R/K312R) E proteins were expressed in *E. coli* system and performed biolayer interferometry (BLI) to measure their binding affinity with Cur-CQDs. A, BLI sensorgrams of Cur-CQDs bound to WT and mutant JEV E recombinant proteins. WT or mutant (S123R, K312R, or S123R/K312R) JEV E recombinant proteins were immobilized on an anti-penta-his (his1k) biosensor and incubated with Cur-CQDs. B, association (k_{on}) and dissociation (k_{off}) rates were measured and calculated using Octet Data Analysis Software 7.0. K_d values were calculated as $K_d = k_{off}/k_{on}$. The standard deviations were calculated from four repeated experiments. Cur-CQDs, Curcumin carbon quantum dots; JEV, Japanese encephalitis virus.

Cur-CQDs. Moreover, we intended to perform the same experiment, a bilayer interferometer, to measure the binding affinity of free guaiacol with WT and mutant E proteins. Unfortunately, the minimum limit for this instrument is a molecular weight of 150 Da, and the molecular weight of free guaiacol is less than 150 Da, so we could not use this instrument. Alternatively, we analyzed the affinity of guaiacol with E protein by isothermal titration calorimetry (ITC), and the K_d of guaiacol with WT E, E-S123R, E-K312R, and E-S123R/K312R were determined to be 4.55×10^{-8} , 2.69×10^{-7} , 2.06×10^{-7} and 5.54×10^{-7} M (Table S3, Supporting information), respectively, revealing that guaiacol exhibited a weaker binding affinity for the mutant E proteins.

Although Cur-CQDs interacted weakly with mutant JEV, the cytopathological effects and viral infectivity of the mutant JEV was found to be much lower than that of WT JEV (Fig. 7). We also applied Cur-CQDs to inhibit two other flaviviruses, dengue virus (DENV) and ZIKV, from infecting BHK-21 cells. We found similar inhibitory effects of Cur-CQDs against JEV and DENV, while no significant antiviral effect was observed against ZIKV (Fig. S7, Supporting information). In addition, we perform the molecular docking of guaiacol with conserved sequences of E protein of DENV and ZIKV (Fig. S8, Supporting information). The binding energies of guaiacol at the two docking positions of domains II and III of DENV's E protein were calculated to be -3.412 and -4.023 kcal mol⁻¹, respectively, which are slightly lower than that of E protein of JEV [-4.746 kcal mol⁻¹ (domain II) and -3.446 kcal mol⁻¹ (domain III)] in average. However, the binding energies of guaiacol to domains II (-3.566 kcal mol⁻¹) and III (-3.554 kcal mol⁻¹) of the E protein of ZIKV were much lower than that of JEV and DENV. Molecular docking results support that Cur-CQDs exhibit potent antiviral activities against JEV and DENV only.

Discussions

No effective treatment for JEV has been found, and only adjuvant therapy and close observation can be used to reduce the symptoms of the disease (49, 50). The JEV vaccine is a

vaccine that prevents Japanese encephalitis. The vaccine is 90% effective in preventing Japanese encephalitis, but the duration of the effect is still unknown, while the effectiveness seems to diminish over time. In addition, there are still some problems with the JEV vaccine. (1) Adults may experience allergic reactions and even shock after JEV vaccination and (2). there is a risk of neurological side effects after JEV vaccination (51, 52). Phytochemicals are considered a safe therapeutic option because no serious side effects have been observed with their use, and many have been found to be well tolerated in animal studies. Therefore, studies on the inhibition of JEV infection by phytochemicals have contributed to the subsequent development of antiviral drugs. Several studies have shown that certain flavonoids can inhibit the effects of flavivirus infection, including quercetin, which can reduce the replication of JEV in host cells and thus inhibit viral infection (53); quercetin can also inhibit the replication process of DENV type 2, thus affecting DENV type 2 infection (54). Naringenin inhibits the late stage of ZIKV infection and inhibits protease activity, thereby affecting ZIKV replication and release (55); in addition, it was shown that naringenin inhibits DENV infection in four different serotypes (56). Luteolin affected the replication and translocation of JEV after infection and reduced viral infection (57); another study reported that luteolin also inhibited dengue fever virus infection (58). One of the flavonoids, Cur, which has also been studied for its ability to inhibit flavivirus infection, for example, Cur dysregulates the ubiquitin-proteasome system and reduces the production of DENV and JEV viral particles (59, 60). Cur binds to ZIKV particles in cells and reduces the viral infection (47). In contrast, Cur is poorly stable and insoluble in water. Therefore, Cur is highly limited in practical applications. We prepared Cur into Cur-CQDs by simple pyrolysis method to improve its water solubility, and in a previous study, we found that Cur-CQDs retained antiviral activity and could effectively inhibit the early and late stages of enterovirus 71 infection, thereby affecting viral infection (13).

In our preliminary study, we found that Cur-CQDs reduced the production of ROS, leading to a decrease in cytotoxicity. Cur is not only an antioxidant (scavenging free radicals) but

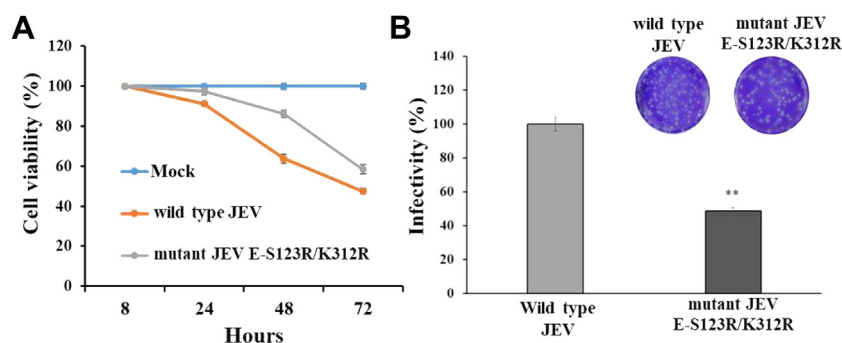


Figure 7. Cur-CQDs-mediated specific attenuation of Japanese encephalitis viral infectivity. A, cytopathological assay of BHK-21 cells infected by WT JEV and mutant JEV E-S123R/K312R. WT JEV or mutant JEV E-S123R/K312R infected BHK-21 cells for 24 h, 48 h, and 72 h, and then cell viability was analyzed by MTT assay. B, plaque assay of BHK-21 cells infected by WT JEV and mutant JEV E-S123R/K312R. WT JEV or mutant JEV E-S123R/K312R infected BHK-21 cells for 72 h, and then viral infectivity was analyzed by plaque assay. Error bars represent the standard deviation of three independent measurements. Asterisks indicate the statistically significant differences in the JEV E-S123R/K312R mutant infection group compared to the WT infection group (** $p < 0.01$). Cur-CQDs, Curcumin carbon quantum dots; JEV, Japanese encephalitis virus.

Antiviral CQDs targeting the JE viral envelope protein

also a prooxidant (generating free radicals) (61). Cur has been reported to produce much greater intracellular ROS than other orthomethoxyphenols such as isoeugenol, bis-eugenol, eugenol, and tetrahydrocurcumin (62). Cur has a conjugated structure consisting of two methoxyphenols and one α,β -unsaturated β -diketone moiety. Cur efficiently produced ROS mainly by autooxidation of the β -diketone moiety itself (62). During pyrolysis, the breakdown of β -diketone derives the formation of CQDs, resulting in the impossibility of inducing intracellular ROS in Cur-CQDs, which leads to apoptosis. The results of the time-of-addition assay showed that Cur-CQDs significantly inhibited the early infection phase of the virus and then affected JEV infection. Cur-CQDs have high solubility and high density of pyrolytic Cur moieties, such as guaiacol and anisole on their surface, which are mainly responsible for their superior antiviral activity (13), so Cur-CQDs can effectively suppress JEV infection.

In experiments to select Cur-CQDs-resistant viruses assay, we found that the E protein S123/K312 of JEV was mutated. The results of TEM and biomolecular interactions analysis indicated that Cur-CQDs would interact with the E protein S123/K312 on JEV particles and then inhibit viral infection. The ectodomain of the JEV E protein consists of three structural domains I, II, and III followed by a flexible stem region that is connected to the C-terminal transmembrane helix (63–65). Two residues, S123 and K312, located near domains II and III of the E protein, respectively, play an important role in viral entry (64). In a neutral environment, the E protein tends to remain on the surface of mature JEV virions in a prefused state (66, 67). Once the E protein is recognized by the membrane receptors of the host cell, JEV can enter the endosome by endocytosis (68). The E protein dimer on the virions is dissociated upon exposure to the low pH of the endosome, initiating fusion (69–73). The stem region of the E protein can facilitate structural extension, allowing insertion of the fusion loop into the host membrane and subsequent homotrimerization of the E protein (69–71). This conformational change leads to juxtaposition of the viral and host cell membranes for interlayer lipid contact, which catalyzes their fusion into a single membrane. As a result, the ribonucleic acid of JEV escapes from the endosome (74). This supports our results that Cur-CQDs bind to the E-S123/K312 sites of the E protein of JEV particles and then inhibit the fusion of the virus with the host cells.

Several studies have found that the membrane fusion ability of the virus is reduced when mutations in amino acids in the E protein were mutated (H144A, H319A, T410A, and Q258A) occur (75). A mutation in amino acid I176R in the E protein of strain JEV SCYA201201 greatly reduced the neurovirulence of the virus in mice (76). In addition, the M279K mutation in the E protein of JEV resulted in restricted viral replication and significantly reduced viremia in monkeys (77). Another report also showed that neurovirulence was significantly reduced after L107F and E138K mutations in the E protein of the JEV SA14 strain (78). In addition, amino acid 123 of the E protein of the JEV-Mie/41/2002 strain was changed from serine to arginine, and virus growth was significantly reduced in

C6/36 cells (79). We infer that the JEV E-S123R/K312R mutant strain is resistant to Cur-CQDs; however, this also results in the mutant virus possessing a weaker fusogenic effect on host cells. Many small molecules have been selected as E protein targets of flavivirus pathogens such as JEV, DENV, and ZIKV, blocking membrane fusion by extracellular exposure of the E protein (80–84). Most of the reported synthetic inhibitors, such as 1662G07, GNF-2, 2,4-disubstituted pyrimidines 2-12-2 and 2,4-disubstituted pyrimidines 7-148-6 have much higher IC_{50} values ($>5 \mu\text{g ml}^{-1}$) than our Cur-CQDs ($0.9 \mu\text{g ml}^{-1}$) (80–84). Furthermore, the selectivity index (CC_{50}/IC_{50}) value of Cur-CQDs (>160) were superior to those of inhibitors (<10) because of their much lower cytotoxicity, suggesting that Cur-CQDs can be used as a highly efficient and biocompatible agent for the prevention of JEV infection (80–84).

We applied Cur-CQDs to inhibit two other flaviviruses, DENV and ZIKV, from infecting BHK-21 cells. Cur-CQDs were found to be effective in inhibiting DENV infection, but not ZIKV infection. Cur and its analogs and derivatives have been reported to have antiviral activity against some flaviviruses such as DENV, ZIKV and chikungunya virus by interfering with virus–host cell binding or viral proteases, even if their selectivity index values are less than 20 (46, 47, 59, 85–87). However, Cur proceeded mainly by inhibiting the attachment of the virus to the host cells. The different antiviral effects can be attributed to the different affinity of Cur-CQDs for the variant E protein structure of flaviviruses. Therefore, more Cur-based carbon nanomaterials should be prepared to broadly inhibit the infections of various viruses.

In summary, the mild carbonization of Cur formed Cur-CQDs with high water solubility and low cytotoxicity, overcoming the thorny problem of Cur limiting its application in various biological fields. The effective binding of Cur-CQDs to JEV greatly reduced the infectivity of the virus in various cells due to the strong inhibition of the early infection stage of the virus. JEV quasispecies resistant to Cur-CQDs possesses two mutant sites in the E protein, K312R and S123R, which play key roles in receptor binding and host cell membrane fusion, respectively. Cur-CQDs bind directly to the E-S123/K312 sites of the E protein or inhibit viral attachment and fusion to host cells by heterotrimerization (Fig. 8). We also found that the mutant JEVs were much less infectious than the WT JEVs. The mild carbonization of Cur and its analogs and derivatives by different methods such as pyrolysis, microwave, hydrothermal, and solvothermal can transform more carbonized Cur-related carbon nanomaterials for antiviral drug development targeting different binding sites of flavivirus E protein. We believe that the combination of clinical antiviral drugs with Cur-based carbon nanomaterials can produce synergistic antiviral effects and improve viral inhibition. In addition, the multiple bioactivities of various Cur-related carbon nanomaterials can be applied to treat inflammation, angiogenesis, tumorigenesis, diabetes, cardiovascular, and neurological-related diseases.

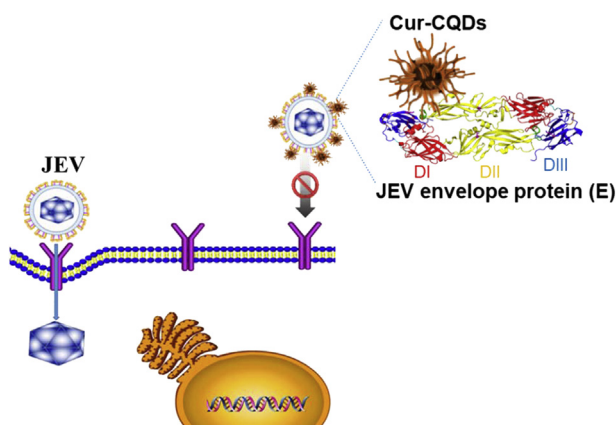


Figure 8. Cur-CQDs inhibit viral attachment and fusion to host cells by binding to the E-S123/K312 sites of the E protein. Cur-CQDs bind directly to the E-S123/K312 sites of the E protein of JEV particle, which then inhibits viral attachment and fusion to the host cell. The mechanism is that Cur-CQDs bind to the E-S123/K312 sites of the E protein, blocking the exposure of the fusion loop structure between domain II and domain III, which in turn inhibits viral fusion. In addition, Cur-CQDs also affect the function of the receptor binding domain on domain III, which then inhibits viral binding to the cells. Cur-CQDs, Curcumin carbon quantum dots; JEV, Japanese encephalitis virus.

Experimental procedures

Materials

Cur powder was purchased from J. T. Baker (Phillipsburg), and the stock solution (10 mM) was prepared in dimethyl sulfoxide (DMSO) and further diluted to the desired concentration with deionized water. DMSO was purchased from Merck KGaA. Sodium chloride, 10X phosphate-buffered saline (PBS) powder, Tris-HCl buffer (1.5 M; pH 7.4), Tris base, glycine, and methanol were purchased from Bio-Future. The N-lauroyl sarcosine sodium salt, formaldehyde solution, ethanol, qPCR reagents, and kits (Kapa Biosystems), cOmplete (EDTA-free protease inhibitor cocktail), dimethyl sulfoxide, sodium phosphate monobasic, anhydrous (NaH_2PO_4), and crystal violet were purchased from Sigma-Aldrich. The para-formaldehyde was purchased from Alfa Aesar. The TRIzol reagent, RevertAid First Strand cDNA Synthesis Kit (Catalog No. K1621), UltraPure Agarose, MicroAmp Fast Reaction Tubes (8 tubes/strip), 3-(4,5-Dimethylthiazol-2-yl)-2,5-diphenyltetrazolium bromide, and T4 DNA Ligase Kit were purchased from ThermoFisher Scientific, Inc. Fetal bovine serum (FBS) was obtained from Gibco BRL. All cell culture media were purchased from Biological Industries. LB Broth Miller, agar, sodium bicarbonate, and sodium dodecyl sulfate were purchased from BioShop Canada. The carbon support film on a 200-mesh copper grid was purchased from Electron Microscopy Sciences. The Octet Anti-Penta-His (HIS1K) BioSensors was purchased from Sartorius. The Ni Sepharose 6 Fast Flow and PD-10 Desalting columns were purchased from GE Healthcare. The BlueRAY Prestained Protein Ladder, PCR Clean-Up and Gel Extraction Kit, Plasmid miniPREP Kit, and Novel Express qPCR System-ROX II were purchased from GeneDireX, Inc. The anti-6X His tag (GTX115045), anti-beta actin (GT5512, GTX629630), goat anti-rabbit IgG secondary antibody [HRP (horseradish peroxidase);

GTX213110-01], and goat anti-mouse IgG secondary antibody (HRP; GTX213111-01) were purchased from GeneTeX. The mouse anti-flavivirus NS3 monoclonal antibody was purchased from Yao-Hong Biotechnology Inc. The 96-well polypropylene microplates (Black; 655209) were purchased from Greiner Bio-One (Kremsmünster, Oberösterreich). The chloroform and sodium phosphate dibasic, anhydrous (Na_2HPO_4) were purchased from J. T. Baker. The Immobilon-P PVDF membrane and Millex-GP Filter (0.22 μm , polyethersulfone, 33 mm) were purchased from Merck Millipore. NANO-WTM was purchased from Nanoprobes. The imidazole, acetic acid, glacial 99%, and 2-propanol were purchased from Panreac Química S.L.U. ACRYL/BIS SOLUTION (30%) 29:1. was purchased from PROTECH (Nankang Software Park). Kanamycin sulfate was purchased from TOKU-E. EasyPrep EndoFree Maxi Plasmid Extraction Kit v2 was purchased from TooLS. The competent cell (catalog #RH217-J40) was purchased from Medical Supply Company Ltd. QuikChange Lightning Site-Directed Mutagenesis Kit was purchased from Agilent Technologies. UltraScience Pico Plus Western Substrate was purchased from Bio-Helix. PBS (containing 137 mM NaCl, 5.0 mM KCl, 0.5 mM CaCl_2 , 1.0 mM MgCl_2 , 10 mM Na_2HPO_4 , and 2.0 mM KH_2PO_4 ; pH 7.4) was used to mimic physiological conditions. Milli-Q ultrapure water (18.2 M Ω cm; EMD Millipore) was used in all experiments.

Cells and virus

The BHK-21 cells (Baby Hamster Kidney cell) were obtained from Ching-lens lab (National Defense Medical Center). The cells were maintained in Roswell Park Memorial Institute (RPMI; Biological Industries) 1640 medium supplemented with 10% FBS in a humidified incubator at 37 °C under 5% CO_2 . JEV T1P1 strain (Wei-June Chen lab, CGU) was propagated in BHK-21 cells and determined the viral titers by plaque assay.

Synthesis of Cur-CQDs

For detailed experimental methods of synthesizing Cur-CQDs, please refer to thermally driven pyrolysis method and described elsewhere (13). Briefly, the Cur powder (20 mg) in a glass vial was heated in a muffle furnace at 180 °C for 2 h to produce brown residues. The residues were cooled to room temperature and dissolved in 5 ml of sodium phosphate buffer (200 mM, pH 12.0). The solution was then sonicated for 1 h, followed by centrifugation at 35,000g for 1 h at 4 °C. The supernatant was then dialyzed through a dialysis membrane (MWCO = 0.5 – 1 KD, Float-A-Lyzer G2, Spectrum Laboratories) against sodium chloride solution (10 mM, ~ 2 L) for 5 h, during which time the sodium chloride solution was changed every 1 h. After 5 h, the sodium chloride solution was replaced with deionized water and dialyzed for 18 h, after which the deionized water was replaced every 6 h during this period. The purified Cur-CQDs solution was stored at 4 °C when not in use. The concentration of the purified Cur-CQDs

Antiviral CQDs targeting the JE viral envelope protein

in the solution (in mg ml⁻¹) was determined by the lyophilization method.

Characterization of Cur-CQDs

The TEM images of Cur-CQDs were recorded using Tecnai G2 F20 S-TWIN (Philips/FEI) systems operating at 200 kV. Before conducting the TEM measurements, the diluted Cur-CQDs (1 mg ml⁻¹) were carefully deposited on a 300-mesh formvar/carbon-coated copper grid, and the excess solvent evaporated at ambient temperature under vacuum. A Synergy 4 multimode microplate spectrophotometer (Biotek Instruments) was used to measure the absorption and photoluminescence properties of the Cur-CQDs. The photoluminescence spectra of as-prepared Cur-CQDs were recorded at excitation wavelengths in the range 325 to 445 nm. The Fourier transform infrared spectrometer (FT/IR-6100, JASCO) was used to analyze functional groups existing in the Cur-CQDs. X-ray diffraction samples were prepared by depositing the Cur-CQD solution on a silicon wafer. X-ray diffraction measurements were performed by using an X-ray diffractometer (D/MAX 2200 VPC, Rigaku, Sendagaya, ShibuyaKu) with the Cu K_{α1} line ($\lambda = 1.54 \text{ \AA}$, energy = 8.8 keV).

Cell viability assay

BHK-21 cells were seeded in 96-well plates at 2×10^4 cells per well, and then the cells were incubated in RPMI 1640 medium containing 2% FBS in the presence of Cur and Cur-CQDs (0 – 1000 $\mu\text{g ml}^{-1}$) for 24 h. The medium was replaced with 3-(4,5-Dimethylthiazol-2-yl)-2,5-diphenyltetrazolium bromide (MTT, Thermo; 50 μl) and incubated at 37 °C for 5 h. DMSO (Merck KGaA; 150 μl) was then added and shaken at 37 °C for 5 min. The absorbance at 570 nm was detected by SpectraMax M2/M2e Microplate Readers (Molecular Device) for cell counting.

Cellular ROS assays

Intracellular ROS formation was assessed by the DCFH-DA assay. DCFH-DA can be deacetylated to the nonfluorescent 2',7'-dichlorodihydrofluorescein by cellular esterases and then oxidized by ROS to fluorescent 2',7'-dichlorodihydrofluorescein with maximum excitation and emission wavelengths of 480 nm and 520 nm, respectively. BHK-21 cell was seeded in 6-well plates (5×10^5 cells per well) and cultured for 24 h for the treatment with Cur (10 $\mu\text{g ml}^{-1}$) or Cur-CQDs (10 $\mu\text{g ml}^{-1}$) for 6 h and then staining with DCFH-DA. We analyze the BHK-21 cell of ROS expression (green fluorescence intensity [500 nm–550 nm]) by fluorescence microscopy.

Plaque assays

BHK-21 cells were cultured in RPMI 1640 medium containing 2% FBS to form a monolayer. To determine the viral titers of JEV, we prepared a serial 10-fold dilutions of the supernatant of JEV-infected medium in serum-free RPMI medium before viral infection. After infection, the cells were overlaid with 2 ml RPMI 1640 medium supplemented with 3% agarose and 10% FBS and then incubated at 37 °C in an

atmosphere of 5% CO₂ for 72 h. Subsequently, the cells were fixed with 4% formaldehyde for 16 h. The JEV-infected cells were then stained with 0.5% crystal violet for 2 min and washed with deionized water. The plaque numbers were counted by visual examination. Virus titers were calculated as the number of plaques with the serial dilution factor and expressed in terms of PFU ml⁻¹.

Antiviral assays

The antiviral efficacy of Cur-CQDs was tested in three stages, including the pretreatment, cotreatment, and post-treatment methods. In the pretreatment assay, Cur-CQDs (100 $\mu\text{g ml}^{-1}$) were added to the cells and left to stand for 2 h at 37 °C. The culture medium containing Cur-CQDs was removed and infected with JEV (MOI=1) for 1 h. The medium containing JEV was then washed twice with PBS, and RPMI 1640 medium containing 10% FBS was added and incubated for 24 h. In the cotreatment experiment, BHK-21 cells were replaced by serum-free RPMI 1640 medium for 2 h. A mixture of JEV (MOI=1) and Cur-CQDs (100 $\mu\text{g ml}^{-1}$) was pre-incubated at 37 °C for 1 h and then added to the cells for 1 h. After that, the medium was removed, washed twice with PBS, replaced with RPMI 1640 medium containing 10% FBS, and incubated at 37 °C for 24 h. In the posttreatment experiment, BHK-21 cell was cultured in serum-free RPMI 1640 medium for 2 h and then infected with JEV (MOI=1) at 37 °C for 1 h. The virus-containing medium was removed and washed twice with PBS. Cells in RPMI 1640 medium were treated with Cur-CQDs (100 $\mu\text{g ml}^{-1}$) for 24 h at 37 °C.

RNA preparation and quantitative real-time PCR

For antiviral assays and viral attachment assays, the total RNA was extracted using TRIzol reagent (Thermo) by following the manufacturer's protocol and cDNA synthesis using RevertAid First Strand cDNA Synthesis Kit (Thermo) according to the manufacturer's instructions, with 500 ng of RNA and the gene-specific reverse primers (Table S4, Supporting information). Quantitative real-time PCR (qPCR) was performed using StepOne (Applied Biosystems) and Novel Express qPCR Reagent (GeneDirex) by following the manufacturer's protocol. Gene-specific primers for qPCR using: JEV NS2a-Fw: GTTTTGGGAGCCTTACTTGT, JEV NS2a-Rv: GCTAAGCATGTTTCATCACTA; mouse GAPDH-Fw, GGCAAGTTCAAAGGCACAGTC, mouse GAPDH-Rv: CACCAGCATCACCCATTT (Table S4).

Western blotting and antisera

The procedures for cell lysates collection and protein separation have been described elsewhere (87). In this study, the primary antibodies used were rabbit anti-JEV NS5 (1: 5,000, Yao-Hong Biotechnology), mouse anti-JEV NS3 (1: 1000 dilutions, Yao-Hong Biotechnology), and mouse anti- β -actin (1: 10,000, GeneTex). The secondary antibodies were anti-mouse antibody (1:5,000, GeneTex) and anti-rabbit antibody (1: 5,000, GeneTex). Targeted signals were visualized using UltraScience Pico Plus Western Substrate (Bio-Helix), and the

images were obtained from the ChemiDoc MP Imaging System (Bio-Rad).

Viral attachment and TEM

BHK-21 cells were treated without or with Cur-CQDs ($100 \mu\text{g ml}^{-1}$) at 37°C or 4°C for 2 h, followed by infected with the JEV (MOI=1) at 4°C for 1 h. The nonattachment virions and Cur-CQDs were removed and washed twice with PBS. The cells were then incubated with RPMI medium supplemented with 10% FBS for an additional 8 or 24 h before fixation. To observe the viral attachment, first, formaldehyde (2%) was added for 5 min to fix the virus–Cur-CQDs ($10 \mu\text{g ml}^{-1}$) mixture, then the mixture ($15 \mu\text{l}$) was dropped on a copper grid (300 mesh). The solution was then drawn out using a filter paper, followed by addition of $15 \mu\text{l}$ 2% NANO-W (Nanoprobes), and washed with $15 \mu\text{l}$ deionized water. The samples were dried overnight under vacuum, and the images were recorded using JEOL JEM 2100PLUS (JEOL, Ltd).

Selection of Cur-CQDs-resistant viruses

BHK-21 cells (5×10^5 cells) were seeded in RPMI 1640 medium containing 2% FBS for 24 h. Serum-free RPMI 1640 medium was used instead for 2 h. Then a mixture of JEV (MOI=1) preincubated with Cur-CQDs ($10 \mu\text{g ml}^{-1}$) was incubated with the cells for 1 h. The cell medium was removed and washed twice with PBS, after which RPMI 1640 medium with 10% FBS was added and incubated for 72 h. The supernatant was then collected and one-tenth of the volume of viral solution was mixed with the Cur-CQDs ($20 \mu\text{g ml}^{-1}$) for 1 h. The cells were then infected for 1 h and replaced with RPMI 1640 medium containing 10% FBS for 72 h. The concentration of Cur-CQDs was gradually increased until $120 \mu\text{g ml}^{-1}$ ($10 \mu\text{g ml}^{-1}$ per passage) following the same procedure. Supernatants of mutant JEVs were collected, and the viral sequences were sequenced using an ABI 3730 DNA analyzer (tri-ibitech). The complete RNA sequences of WT and mutant type JEV were aligned and compared using Multiple Sequence Alignment (CLUSTALW).

Construction of transgenic vectors and site-directed mutagenesis

JEV RNA was prepared using TRIzol reagent (Thermo) and cDNA synthesis using RevertAid First Strand cDNA Synthesis Kit (Thermo) according to the manufacturer's protocol, with 500 ng of RNA and JEV NS1-specific reverse primers: GCCGCTCGAGTCATTCACCATTAAGCATC (Table S4). The E segment of JEV was performed using 2X Go Taq Green Master Mix (Promega Corporation) and Gene-specific primers: E-FW: ATTAGGTACCGCCACCATGGGCTTTAA TTGTCTGGGAAT, E-RV: GGC GCGAATTCAGCATGCA CATTGGTTCGCTAAGAACACG (the underlined letters in the forward and reverse primers indicate *Kpn* I and *Eco*RI restriction enzyme sites, respectively) (Table S4) and following the manufacturer's protocol to amplify the target gene by PCR (ABI veriti 96 well thermal cycler, Applied Biosystems). The target DNA was purified by gel extraction kit (GeneDireX). Subsequently, the

target DNA and pET-30(a)+ vector was respectively digested by the restriction enzyme of *Kpn* I and *Eco*RI. Then, the enzyme-digested fragments were purified by gel extraction kit (GeneDireX) and ligated together by T4 ligation kit (Thermo). The ligated product was subsequently transformed to *E. coli* DH5 α strain and screened with kanamycin (88). The constructed pET30a (+) plasmids containing the E segment of JEV (designated as pET30a(+)-E). The pET30a(+)-E-Mut-S123R, pET30a(+)-E-Mut-K312R, and pET30a(+)-E-Mut-S123R/K312R were produced using QuikChange Lightning Site-Directed Mutagenesis Kit (Agilent) by following the manufacturer's protocol (89).

Recombinant protein preparation and purification

The pET-JEV E, pET-E-Mut-S123R, pET-E-Mut-K312R, and pET-E-Mut-S123R/K312R plasmids respectively transformed into *E. coli* BL21 (Medical Supply Company Ltd) and induced target protein expression by 0.6 mM isopropyl β -D-1-thiogalactopyranoside in Luria-Bertani (LB) medium containing kanamycin (final concentration: $50 \mu\text{g ml}^{-1}$) at 25°C for 16 h. His-JEV E recombinant protein and the other proteins with mutation sites were purified by column chromatography on Ni sepharose 6 fast flow (GE Healthcare). The induction and purification of recombinant protein refer to the manufacturer's protocol and previous studies (89).

Biomolecular interactions analysis

The Octet RED96 (FortéBio) was used to analyze the interaction between Cur-CQDs and WT and mutant type JEV envelope proteins (E proteins). Five His antibody-coated probes (Sartorius) were immersed in PBS containing 0.1 mg ml^{-1} BSA (Sigma-Aldrich) for 30 min, and then, the probes were washed back and forth with 10 mM Glycine-HCl (pH 1.5) followed by washing three times with PBS containing 0.1 mg ml^{-1} BSA. The probe was then incubated in PBS containing 0.1 mg ml^{-1} BSA for 10 min to obtain equilibrium and then incubated for 10 min into the sample group (His-tag JEV E proteins: WT, S123R, K312R, or S123R/K312R). The His-tag sample was bound to the probe and then incubated in PBS containing 0.1 mg ml^{-1} BSA and washed for 10 min (to remove unbound His-tag JEV E proteins). The probe was then equilibrated in PBS containing 0.1 mg ml^{-1} BSA for 10 min and then incubated with Cur-CQDs ($10 \mu\text{g ml}^{-1}$) for 10 min to determine the association rate constant (K_{on}). Subsequently, the probe was placed in PBS containing 0.1 mg ml^{-1} BSA to determine the dissociation rate constant (K_{off}). The dissociation constant (K_{d}) values were calculated as $k_{\text{off}}/k_{\text{on}}$.

Isothermal titration calorimetry

All ITC measurements were carried out at 25°C with the Affinity ITC calorimeter (TA Instruments) to measure the binding affinity of guaiacol and JEV E proteins using 100 rpm stirring and succeeding injection of guaiacol solution into the sample cell coating JEV E proteins. The Cur-CQDs and JEV E proteins were prepared in a 20 mM sodium phosphate buffer solution (pH 7.4) containing 100 mM NaCl and 10 mM imidazole, respectively. Guaiacol ($3.0 \mu\text{M}$) and JEV E proteins

Antiviral CQDs targeting the JE viral envelope protein

(10 μ M) were loaded into the syringe and the sample cell (182 μ l), respectively. Cur-CQDs (1.0 μ l) was injected every 200 s until the JEV E proteins were saturated (a total of 30 injections). The data from the entire titration curve were processed with the standard NanoAnalyze software package (version 3.12.0). The software was used to calculate enthalpy (ΔH), entropy (ΔS), and the equilibrium constant ($1/K_d$). Gibbs free energy (ΔG) was calculated using the equation: $\Delta G = \Delta H - T\Delta S$

Docking methodology and procedure

In terms of softwares used, the molecular docking including ligand and protein preparation was done by Schrodinger Release 2021-3 (Maestro Version 12.9.123). The ligand preparation was done by LigPrep. The protein preparation was done by Protein Preparation Wizard (MODELLER 10.1). In terms of protein and ligand preparation, guaiacol (DB11359) was obtained from DrugBank and optimized by using the LigPrep procedure. The E protein (3p54) was obtained from Protein Data Bank (PDB) and removed water molecules, and the 3p54 has used a template as mutant type (S123R and K312R) from MODELLER 10.1. All residues of E protein were optimized the energy minimization by using the solvation model (VSGB) and force field (OPLS4) in Prime. In terms of docking procedure, Glide ligand docking was employed for docking simulations. The affinity grid maps preparation was defined guaiacol as grid box size (20 Å) with a ligand diameter midpoint box (10 Å). The box center of the grid box was separately located at the centroid of residue 123 or 312. Cluster analysis was performed on the docked results using an RMS tolerance of 2.0 Å. Finally, the more energetically favorable 10 cluster poses were evaluated by using Python Molecule Viewer (PMV ver.1.5.6) and PyMOL ver.1.1.7 (DeLano Scientific LLC).

Statistical analysis

All experiments were independently repeated three or four times. The values were expressed as the mean \pm standard deviation (SD). Statistical analysis was performed using a one-way ANOVA test to compare the differences in test values between the treatment and virus control group. Statistical significance is represented by asterisks in the figures as follows: * $p < 0.05$, ** $p < 0.01$, *** $p < 0.001$.

Data availability

All relevant data are available upon request from the main text and supporting information.

Supporting information—This article contains supporting information (89).

Author contributions—H-H. C. and A. A. conceptualization; C-J. L., H-Y. L., and Y-J. T. methodology; J-Y. M. and P-H. W. formal analysis; R. W. and C-C. H. investigation; W-S. T., H-J. L., H. Y. L., Y-J. T., and A. A. resources; C-C. H. and H-J. L. data curation; R. W.

and C-C. H. supervision; R. W. and C-C. H. funding acquisition; H-H. C., W-S. T., H-J. L., H. Y. L., Y-J. T., C-J. L., J-Y. M., P-H. W., R. W. and A. A. writing-review and editing; W-S. T., writing-original draft.

Funding and additional information—This study was supported by the Ministry of Science and Technology of Taiwan under Contract Nos. 110 to 2221-E-019 to 001, 110 to 2320-B-182 to 029 and 110 to 2811-M-019 to 501, by Chang Gung memorial hospital research fund (CMRPD1H0321–3, CMRPD1K0251–2 and CMRPD1L0061) and by the Center of Excellence for the Oceans, National Taiwan Ocean University from The Featured Areas Research Center Program within the framework of the Higher Education Sprout Project by the Ministry of Education (MOE) in Taiwan.

Conflict of interest—The authors declare that they have no conflicts of interest with the contents of this article.

Abbreviations—The abbreviations used are: BHK-21, Baby hamster kidney; BSA, Bovine serum albumin; Cur-CQDs, curcumin carbon quantum dots; DENV, Dengue virus; FBS, Fetal Bovine Serum; HEK, human embryonic kidney; HRTEM, high resolution transmission electron microscopy; ITC, isothermal titration calorimetry; JEV, Japanese encephalitis virus; NS, nonstructural protein; PBS, Phosphate buffered saline; qPCR, quantitative real-time PCR; ROS, reactive oxygen species; SD, standard deviation; TEM, transmission electron microscopy; Vero, monkey kidney epithelial; ZIKV, Zika virus.

References

1. Hansen, V., Oren, E., Dennis, L. K., and Brown, H. E. (2016) Infectious disease mortality trends in the United States, 1980–2014. *JAMA* **316**, 2149–2151
2. Chakravarty, M., and Vora, A. (2021) Nanotechnology-based antiviral therapeutics. *Drug Deliv. Transl. Res.* **11**, 748–787
3. Jackman, J. A., Yoon, B. K., Ouyang, L., Wang, N., Ferhan, A. R., Kim, J., Majima, T., and Cho, N. J. (2021) Biomimetic nanomaterial strategies for virus targeting: Antiviral therapies and vaccines. *Adv. Funct. Mater.* **31**, 2008352
4. Zhou, J., Krishnan, N., Jiang, Y., Fang, R. H., and Zhang, L. (2021) Nanotechnology for virus treatment. *Nano Today* **36**, 101031
5. Yoon, B. K., Jeon, W.-Y., Sut, T. N., Cho, N.-J., and Jackman, J. A. (2020) Stopping membrane-enveloped viruses with nanotechnology strategies: Toward antiviral drug development and pandemic preparedness. *ACS Nano* **15**, 125–148
6. Osminkina, L. A., Agafilushkina, S. N., Kropotkina, E. A., Saushkin, N. Y., Bozhev, I. V., Abramchuk, S. S., Samsonova, J. V., and Gambaryan, A. S. (2022) Antiviral adsorption activity of porous silicon nanoparticles against different pathogenic human viruses. *Bioact. Mater.* **7**, 39–46
7. Das, C., Paul, S. S., Saha, A., Singh, T., Saha, A., Im, J., and Biswas, G. (2020) Silver-based nanomaterials as therapeutic agents against coronaviruses: A review. *Int. J. Nanomedicine* **15**, 9301
8. Tortella, G., Rubilar, O., Fincheira, P., Pieretti, J. C., Duran, P., Lourenço, I. M., and Seabra, A. B. (2021) Bactericidal and virucidal activities of biogenic metal-based nanoparticles: Advances and perspectives. *Antibiotics* **10**, 783
9. Skalny, A. V., Rink, L., Ajsuvakova, O. P., Aschner, M., Gritsenko, V. A., Alekseenko, S. I., Svistunov, A. A., Petrakis, D., Spandidos, D. A., and Aaseth, J. (2020) Zinc and respiratory tract infections: Perspectives for COVID-19. *Int. J. Mol. Med.* **46**, 17–26
10. Pilaquinga, F., Morey, J., Torres, M., Seqqat, R., and Piña, M.d.I.N. (2021) Silver nanoparticles as a potential treatment against SARS-CoV-2: A review. *Wiley Interdiscip. Rev. Nanomed. Nanobiotechnol.* **13**, e1707
11. Serrano-Aroca, Á., Takayama, K., Tuñón-Molina, A., Seyran, M., Hassan, S. S., Pal Choudhury, P., Uversky, V. N., Lundstrom, K., Adadi, P., and

- Palù, G. (2021) Carbon-based nanomaterials: Promising antiviral agents to combat COVID-19 in the microbial-resistant era. *ACS Nano* **15**, 8069–8086
12. Innocenzi, P., and Stagi, L. (2020) Carbon-based antiviral nanomaterials: Graphene, C-dots, and fullerenes. A perspective. *Chem. Sci.* **11**, 6606–6622
 13. Lin, C. J., Chang, L., Chu, H. W., Lin, H. J., Chang, P. C., Wang, R. Y., Unnikrishnan, B., Mao, J. Y., Chen, S. Y., and Huang, C. C. (2019) High amplification of the antiviral activity of curcumin through transformation into carbon quantum dots. *Small* **15**, e1902641
 14. Ye, S., Shao, K., Li, Z., Guo, N., Zuo, Y., Li, Q., Lu, Z., Chen, L., He, Q., and Han, H. (2015) Antiviral activity of graphene oxide: How sharp edged structure and charge matter. *ACS Appl. Mater. Interfaces* **7**, 21571–21579
 15. Unal, M. A., Bayrakdar, F., Nazir, H., Besbinar, O., Gurcan, C., Lozano, N., Arellano, L. M., Yalcin, S., Panatli, O., and Celik, D. (2021) Graphene oxide nanosheets interact and interfere with SARS-CoV-2 surface proteins and cell receptors to inhibit infectivity. *Small* **17**, e2101483
 16. Martinez, Z. S., Castro, E., Seong, C.-S., Cerón, M. R., Echegoyen, L., and Llano, M. (2016) Fullerene derivatives strongly inhibit HIV-1 replication by affecting virus maturation without impairing protease activity. *Antimicrob. Agents Chemother.* **60**, 5731–5741
 17. Falynskova, I., Ionova, K., Dedova, A., Leneva, I., Makhmudova, N., and Rasnetsov, L. (2014) Antiviral activity of fullerene-(tris-aminocaproic acid) hydrate against respiratory syncytial virus in HEP-2 cell culture. *Pharm. Chem. J.* **48**, 85–88
 18. Kataoka, H., Ohe, T., Takahashi, K., Nakamura, S., and Mashino, T. (2016) Novel fullerene derivatives as dual inhibitors of hepatitis C virus NS5B polymerase and NS3/4A protease. *Med. Chem. Lett.* **26**, 4565–4567
 19. Klimova, R., Andreev, S., Momotyuk, E., Demidova, N., Fedorova, N., Chernoryzh, Y., Yurlov, K., Turetskiy, E., Baraboshkina, E., and Sher-shakova, N. (2020) Aqueous fullerene C60 solution suppresses herpes simplex virus and cytomegalovirus infections. *Fuller. Nanotub. Carbon Nanostruct.* **28**, 487–499
 20. Ramos-Soriano, J., Reina, J. J., Illescas, B. M., De La Cruz, N., Rodriguez-Perez, L., Lasala, F., Rojo, J., Delgado, R., and Martin, N. (2019) Synthesis of highly efficient multivalent disaccharide/[60] fullerene nanoballs for emergent viruses. *J. Am. Chem. Soc.* **141**, 15403–15412
 21. Tollas, S., Bereczki, I., Borbás, A., Batta, G., Vanderlinden, E., Naesens, L., and Herczegh, P. (2014) Synthesis of a cluster-forming sialylthio-D-galactose fullerene conjugate and evaluation of its interaction with influenza virus hemagglutinin and neuraminidase. *Bioorg. Med. Chem. Lett.* **24**, 2420–2423
 22. Mostafavi, S., Mehrnia, M., and Rashidi, A. (2009) Preparation of nanofilter from carbon nanotubes for application in virus removal from water. *Desalination* **238**, 271–280
 23. Barras, A., Pagneux, Q., Sane, F., Wang, Q., Boukherroub, R., Hober, D., and Szunerits, S. (2016) High efficiency of functional carbon nanodots as entry inhibitors of herpes simplex virus type 1. *ACS Appl. Mater. Inter.* **8**, 9004–9013
 24. Du, T., Liang, J., Dong, N., Liu, L., Fang, L., Xiao, S., and Han, H. (2016) Carbon dots as inhibitors of virus by activation of type I interferon response. *Carbon* **110**, 278–285
 25. Garg, P., Sangam, S., Kochhar, D., Pahari, S., Kar, C., and Mukherjee, M. (2020) Exploring the role of triazole functionalized heteroatom Co-doped carbon quantum dots against human coronaviruses. *Nano Today* **35**, 101001
 26. Iannazzo, D., Pistone, A., Ferro, S., De Luca, L., Monforte, A. M., Romeo, R., Buemi, M. R., and Pannecouque, C. (2018) Graphene quantum dots based systems as HIV inhibitors. *Bioconjug. Chem.* **29**, 3084–3093
 27. Tong, T., Hu, H., Zhou, J., Deng, S., Zhang, X., Tang, W., Fang, L., Xiao, S., and Liang, J. (2020) Glycyrrhizic-acid-based carbon dots with high antiviral activity by multisite inhibition mechanisms. *Small* **16**, 1906206
 28. Liu, J., Li, R., and Yang, B. (2020) Carbon dots: A new type of carbon-based nanomaterial with wide applications. *ACS Cent. Sci.* **6**, 2179–2195
 29. Turtle, L., and Solomon, T. (2018) Japanese Encephalitis—The prospects for new treatments. *Nat. Rev. Neurol.* **14**, 298–313
 30. Mansfield, K. L., Hernández-Triana, L. M., Banyard, A. C., Fooks, A. R., and Johnson, N. (2017) Japanese encephalitis virus infection, diagnosis and control in domestic animals. *Vet. Microbiol.* **201**, 85–92
 31. Carro, S. D., and Cherry, S. (2021) Beyond the surface: Endocytosis of mosquito-borne flaviviruses. *Viruses* **13**, 13
 32. Zeng, Q., Feng, T., Tao, S., Zhu, S., and Yang, B. (2021) Precursor-dependent structural diversity in luminescent carbonized polymer dots (CPDs): The nomenclature. *Light Sci. Appl.* **10**, 142
 33. Aparicio, J. A. C., Ponce, H., and Rudamas, C. (2020) Interlayer transition in graphene carbon quantum dots. *MRS Adv.* **5**, 3345–3352
 34. Nelson, K. M., Dahlin, J. L., Bisson, J., Graham, J., Pauli, G. F., and Walters, M. A. (2017) The essential medicinal chemistry of curcumin: Miniperspective. *J. Med. Chem.* **60**, 1620–1637
 35. Nelson, K. M., Dahlin, J. L., Bisson, J., Graham, J., Pauli, G. F., and Walters, M. A. (2017) Curcumin may (not) defy science. *ACS Med. Chem. Lett.* **8**, 467–470
 36. Yang, X. X., Li, C. M., Li, Y. F., Wang, J., and Huang, C. Z. (2017) Synergistic antiviral effect of curcumin functionalized graphene oxide against respiratory syncytial virus infection. *Nanoscale* **9**, 16086–16092
 37. Yang, X. X., Li, C. M., and Huang, C. Z. (2016) Curcumin modified silver nanoparticles for highly efficient inhibition of respiratory syncytial virus infection. *Nanoscale* **8**, 3040–3048
 38. Woo, J.-H., Kim, Y.-H., Choi, Y.-J., Kim, D.-G., Lee, K.-S., Bae, J. H., Min, D. S., Chang, J.-S., Jeong, Y.-J., and Lee, Y. H. (2003) Molecular mechanisms of curcumin-induced cytotoxicity: Induction of apoptosis through generation of reactive oxygen species, down-regulation of bcl-X L and IAP, the release of cytochrome C and inhibition of akt. *Carcinogenesis* **24**, 1199–1208
 39. Takegami, T., Sakamuro, D., and Furukawa, T. (1995) Japanese encephalitis virus nonstructural protein NS3 has RNA binding and ATPase activities. *Virus Genes* **9**, 105–112
 40. Edward, Z., and Takegami, T. (1993) Localization and functions of Japanese encephalitis virus nonstructural proteins NS3 and NS5 for viral RNA synthesis in the infected cells. *Microbiol. Immunol.* **37**, 239–243
 41. Brooks, A. J., Johansson, M., John, A. V., Xu, Y., Jans, D. A., and Vasudevan, S. G. (2002) The interdomain region of dengue NS5 protein that binds to the viral helicase NS3 contains independently functional importin β 1 and importin α/β -recognized nuclear localization signals. *J. Biol. Chem.* **277**, 36399–36407
 42. Li, K., Phoo, W. W., and Luo, D. (2014) Functional interplay among the flavivirus NS3 protease, helicase, and cofactors. *Virology* **29**, 74–85
 43. Du, T., Lu, J., Liu, L., Dong, N., Fang, L., Xiao, S., and Han, H. (2018) Antiviral activity of graphene oxide–silver nanocomposites by preventing viral entry and activation of the antiviral innate immune response. *ACS Appl. Bio. Mater.* **1**, 1286–1293
 44. Fahmi, M., Sukmayani, W., Khairunisa, S. Q., Witaningrum, A., Indriati, D., Matondang, M., Chang, J.-Y., Kotaki, T., and Kameoka, M. (2016) Design of boronic acid–attributed carbon dots on inhibits HIV-1 entry. *RSC Adv.* **6**, 92996–93002
 45. Ziem, B., Azab, W., Gholami, M., Rabe, J. P., Osterrieder, N., and Haag, R. (2017) Size-dependent inhibition of herpesvirus cellular entry by polyvalent nanoarchitectures. *Nanoscale* **9**, 3774–3783
 46. Balasubramanian, A., Pilankatta, R., Teramoto, T., Sajith, A. M., Nwulia, E., Kulkarni, A., and Padmanabhan, R. (2019) Inhibition of dengue virus by curcuminoids. *Antivir. Res.* **162**, 71–78
 47. Mounce, B. C., Cesaro, T., Carrau, L., Vallet, T., and Vignuzzi, M. (2017) Curcumin inhibits Zika and chikungunya virus infection by inhibiting cell binding. *Antivir. Res.* **142**, 148–157
 48. Baikerikar, S. (2017) Curcumin and natural derivatives inhibit ebola viral proteins: An in silico approach. *Pharmacogn. Res.* **9**, S15–S22
 49. Solomon, T., Dung, N. M., Kneen, R., Gainsborough, M., Vaughn, D. W., and Khanh, V. T. (2000) Japanese encephalitis. *JNNP* **68**, 405–415
 50. Iro, M. A., Martin, N. G., Absoud, M., and Pollard, A. J. (2017) Intravenous immunoglobulin for the treatment of childhood encephalitis. *CDSR* **10**, CD011367
 51. Jelinek, T. (2008) Japanese encephalitis vaccine in travelers. *Expert Rev. Vaccin.* **7**, 689–693

Antiviral CQDs targeting the JE viral envelope protein

52. Kurane, I., and Takasaki, T. (2000) Immunogenicity and protective efficacy of the current inactivated Japanese encephalitis vaccine against different Japanese encephalitis virus strains. *Vaccine* **18**, 33–35
53. Johari, J., Kianmehr, A., Mustafa, M. R., Abubakar, S., and Zandi, K. (2012) Antiviral activity of baicalein and quercetin against the Japanese encephalitis virus. *Int. J. Mol. Sci.* **13**, 16785–16795
54. Zandi, K., Lim, T.-H., Rahim, N.-A., Shu, M.-H., Teoh, B.-T., Sam, S.-S., Danlami, M.-B., Tan, K.-K., and Abubakar, S. (2013) Extract of scutellaria baicalensis inhibits dengue virus replication. *BMC Complement Altern. Med.* **13**, 91
55. de Oliveira Mendes, L. A., Ponciano, C. S., Cataneo, A. H. D., Wowk, P. F., Bordignon, J., Silva, H., de Almeida, M. V., and Ávila, E. P. (2020) The anti-Zika virus and anti-tumoral activity of the citrus flavanone lipophilic naringenin-based compounds. *Chem. Biol. Interact.* **331**, 109218
56. Frabasile, S., Koishi, A. C., Kuczera, D., Silveira, G. F., Verri, W. A., Jr., Dos Santos, C. N. D., and Bordignon, J. (2017) The citrus flavanone naringenin impairs dengue virus replication in human cells. *Sci. Rep.* **7**, 41864
57. Fan, W., Qian, S., Qian, P., and Li, X. (2016) Antiviral activity of luteolin against Japanese encephalitis virus. *Virus Res.* **220**, 112–116
58. Peng, M., Watanabe, S., Chan, K. W. K., He, Q., Zhao, Y., Zhang, Z., Lai, X., Luo, D., Vasudevan, S. G., and Li, G. (2017) Luteolin restricts dengue virus replication through inhibition of the proprotein convertase furin. *Antivir. Res.* **143**, 176–185
59. Padilla-s, L., Rodríguez, A., Gonzales, M. M., Gallego-g, J. C., and Castaño-o, J. C. (2014) Inhibitory effects of curcumin on dengue virus type 2-infected cells *in Vitro*. *Arch. Virol.* **159**, 573–579
60. Dutta, K., Ghosh, D., and Basu, A. (2009) Curcumin protects neuronal cells from Japanese encephalitis virus-mediated cell death and also inhibits infective viral particle formation by dysregulation of ubiquitin–proteasome system. *J. Neuroimmune Pharmacol.* **4**, 328–337
61. Ahsan, H., Parveen, N., Khan, N. U., and Hadi, S. (1999) Pro-oxidant, antioxidant and cleavage activities on DNA of curcumin and its derivatives demethoxycurcumin and bisdemethoxycurcumin. *Chem. Biol. Interact.* **121**, 161–175
62. Fujisawa, S., Atsumi, T., Ishihara, M., and Kadoma, Y. (2004) Cytotoxicity, ROS-generation activity and radical-scavenging activity of curcumin and related compounds. *Anticancer Res.* **24**, 563–570
63. Luca, V. C., AbiMansour, J., Nelson, C. A., and Fremont, D. H. (2012) Crystal structure of the Japanese encephalitis virus envelope protein. *J. Virol.* **86**, 2337–2346
64. Hu, T., Wu, Z., Wu, S., Chen, S., and Cheng, A. (2021) The key amino acids of E protein involved in early flavivirus infection: Viral entry. *Virol. J.* **18**, 136
65. Wang, X., Li, S.-H., Zhu, L., Nian, Q.-G., Yuan, S., Gao, Q., Hu, Z., Ye, Q., Li, X.-F., and Xie, D.-Y. (2017) Near-atomic structure of Japanese encephalitis virus reveals critical determinants of virulence and stability. *Nat. Commun.* **8**, 14
66. Zhang, Y., Zhang, W., Ogata, S., Clements, D., Strauss, J. H., Baker, T. S., Kuhn, R. J., and Rossmann, M. G. (2004) Conformational changes of the flavivirus E glycoprotein. *Structure* **12**, 1607–1618
67. Modis, Y., Ogata, S., Clements, D., and Harrison, S. C. (2003) A ligand-binding pocket in the dengue virus envelope glycoprotein. *Proc. Natl. Acad. Sci. U. S. A.* **100**, 6986–6991
68. Yun, S.-I., and Lee, Y.-M. (2018) Early events in Japanese encephalitis virus infection: Viral entry. *Pathogens* **7**, 68
69. Allison, S. L., Schalich, J., Stiasny, K., Mandl, C. W., Kunz, C., and Heinz, F. X. (1995) Oligomeric rearrangement of tick-borne encephalitis virus envelope proteins induced by an acidic pH. *J. Virol.* **69**, 695–700
70. Heinz, F. X., and Allison, S. L. (2000) Structures and mechanisms in flavivirus fusion. *Adv. Virus Res.* **55**, 231–269
71. Stiasny, K., Allison, S. L., Schalich, J., and Heinz, F. X. (2002) Membrane interactions of the tick-borne encephalitis virus fusion protein E at low pH. *J. Virol.* **76**, 3784–3790
72. Fritz, R., Stiasny, K., and Heinz, F. X. (2008) Identification of specific histidines as pH sensors in flavivirus membrane fusion. *J. Cell Biol.* **183**, 353–361
73. Nayak, V., Dessau, M., Kucera, K., Anthony, K., Ledizet, M., and Modis, Y. (2009) Crystal structure of dengue virus type 1 envelope protein in the postfusion conformation and its implications for membrane fusion. *J. Virol.* **83**, 4338–4344
74. Nour, A. M., Li, Y., Wolenski, J., and Modis, Y. (2013) Viral membrane fusion and nucleocapsid delivery into the cytoplasm are distinct events in some flaviviruses. *PLoS Pathog.* **9**, e1003585
75. Liu, H., Liu, Y., Wang, S., Zhang, Y., Zu, X., Zhou, Z., Zhang, B., and Xiao, G. (2015) Structure-based mutational analysis of several sites in the E protein: Implications for understanding the entry mechanism of Japanese encephalitis virus. *J. Virol.* **89**, 5668
76. Zhou, Y., Wu, R., Zhao, Q., Chang, Y.-F., Wen, X., Feng, Y., Huang, X., Wen, Y., Yan, Q., and Huang, Y. (2018) Mutation of I176R in the E coding region weakens Japanese encephalitis virus neurovirulence, but not its growth rate in BHK-21 cells. *Arch. Virol.* **163**, 1351–1355
77. Monath, T. P., Arroyo, J., Levenbook, I., Zhang, Z.-X., Catalan, J., Draper, K., and Guirakhoo, F. (2002) Single mutation in the flavivirus envelope protein hinge region increases neurovirulence for mice and monkeys but decreases viscerotropism for monkeys: Relevance to development and safety testing of live, attenuated vaccines. *J. Virol.* **76**, 1932–1943
78. Yang, J., Yang, H., Li, Z., Wang, W., Lin, H., Liu, L., Ni, Q., Liu, X., Zeng, X., and Wu, Y. (2017) Envelope protein mutations L107F and E138K are important for neurovirulence attenuation for Japanese encephalitis virus SA14-14-2 strain. *Viruses* **9**, 20
79. Yamaguchi, Y., Nukui, Y., Kotaki, A., Sawabe, K., Saijo, M., Watanabe, H., Kurane, I., Takasaki, T., and Tajima, S. (2013) Characterization of a serine-to-asparagine substitution at position 123 in the Japanese encephalitis virus E protein. *J. Gen. Virol.* **94**, 90–96
80. Clark, M. J., Miduturu, C., Schmidt, A. G., Zhu, X., Pitts, J. D., Wang, J., Potisopon, S., Zhang, J., Wojciechowski, A., and Chu, J. J. H. (2016) GNF-2 inhibits dengue virus by targeting abl kinases and the viral E protein. *Cell Chem. Biol.* **23**, 443–452
81. de Wispelaere, M., Lian, W., Potisopon, S., Li, P.-C., Jang, J., Ficarro, S. B., Clark, M. J., Zhu, X., Kaplan, J. B., and Pitts, J. D. (2018) Inhibition of flaviviruses by targeting a conserved pocket on the viral envelope protein. *Cell Chem. Biol.* **25**, 1006–1016.e8
82. Li, P.-C., Jang, J., Hsia, C.-Y., Grooms, P. V., Lian, W., de Wispelaere, M., Pitts, J. D., Wang, J., Kwiatkowski, N., and Gray, N. S. (2019) Small molecules targeting the flavivirus E protein with broad-spectrum activity and antiviral efficacy *in vivo*. *ACS Infect. Dis.* **5**, 460–472
83. Lian, W., Jang, J., Potisopon, S., Li, P.-C., Rahmeh, A., Wang, J., Kwiatkowski, N. P., Gray, N. S., and Yang, P. L. (2018) Discovery of immunologically inspired small molecules that target the viral envelope protein. *ACS Infect. Dis.* **4**, 1395–1406
84. Schmidt, A. G., Lee, K., Yang, P. L., and Harrison, S. C. (2012) Small-molecule inhibitors of dengue-virus entry. *PLoS Pathog.* **8**, e1002627
85. Kim, M., Choi, H., and Kim, Y. B. (2021) Therapeutic targets and biological mechanisms of action of curcumin against Zika virus: *In silico* and *in Vitro* analyses. *Eur. J. Pharmacol.* **904**, 174144
86. Pacho, M. N., Pagni, E. N., Díaz Sierra, J. B., Morell, M. L., Sepúlveda, C. S., Damonte, E. B., García, C. C., and D'Accorso, N. B. (2021) Antiviral activity against Zika virus of a new formulation of curcumin in poly lactic-Co-glycolic acid nanoparticles. *J. Pharm. Pharmacol.* **73**, 357–365
87. Wu, Y.-P., Chang, C.-M., Hung, C.-Y., Tsai, M.-C., Schuyler, S. C., and Wang, R. Y.-L. (2011) Japanese encephalitis virus Co-opts the ER-stress response protein GRP78 for viral infectivity. *Virol. J.* **8**, 128
88. Wang, R. Y., Kuo, R.-L., Ma, W.-C., Huang, H.-I., Yu, J.-S., Yen, S.-M., Huang, C.-R., and Shih, S.-R. (2013) Heat shock protein-90-beta facilitates enterovirus 71 viral particles assembly. *Virology* **443**, 236–247
89. Hiraga, K., Mejzlik, P., Marcisin, M., Vostrosablin, N., Gromek, A., Arnold, J., Wiewiora, S., Svarba, R., Prihoda, D., and Clarova, K. (2021) Mutation maker, an open source oligo design platform for protein engineering. *ACS Synth. Biol.* **10**, 357–370